A Phenylnorstatine Inhibitor Binding to HIV-1 Protease: Geometry, Protonation, and Subsite−Pocket Interactions Analyzed at Atomic Resolution

Jiri Brynda,*,† Pavlina Rezacova,† Milan Fabry,† Magdalena Horejsi,† Renata Stouracova,† Juraj Sedlacek,† Milan Soucek,‡ Martin Hradilek,‡ Martin Lepsik,‡ and Jan Konvalinka‡

Institute of Molecular Genetics, Academy of Sciences of the Czech Republic, Flemingovo nám. 2, 16637 Prague 6, Czech Republic, and Institute of Organic Chemistry and Biochemistry, Academy of Sciences of the Czech Republic, Flemingovo nám. 2, 16610 Prague 6, Czech Republic

Received November 18, 2003

The X-ray structure of a complex of HIV-1 protease (PR) with a phenylnorstatine inhibitor Z-Pns-Phe-Glu-Glu-NH_2 has been determined at 1.03 Å, the highest resolution so far reported for any HIV PR complex. The inhibitor shows subnanomolar K_i values for both the wild-type PR and the variant representing one of the most common mutations linked to resistance development. The structure comprising the phenylnorstatine moiety of (2*R*,3*S*)-chirality displays a unique pattern of hydrogen bonding to the two catalytic aspartate residues. This high resolution makes it possible to assess the donor and acceptor relations of this hydrogen bonding and to indicate a proton shared by the two catalytic residues. A structural mechanism for the unimpaired inhibition of the protease Val82Ala mutant is also suggested, based on energy calculations and analyses.

Introduction

A structure-aided design of HIV protease (PR) inhibitors has led to a class of drugs useful in clinical anti-HIV intervention (see ref 1 for review). Nevertheless, mutational development of HIV PR drug resistance presents a major medical complication. Thus, the present state of anti-AIDS therapies calls for the design of novel compounds that would overcome the problem of HIV PR resistance to current drugs. Inhibitors with unconventional binding modes (or those interacting with HIV PR domains other than the active site, e.g., the dimerization domain[2]) might open a way to a new generation of anti-HIV PR compounds capable of inhibiting drug-resistant enzyme species (e.g., refs 3−6).

Recently, a combinatorial chemistry approach[7] yielded a series of novel pluripotent HIV PR inhibitors having a picomolar range for their K_i values for the wild-type HIV PR as well as various degrees of insensitivity of their inhibitory potency to HIV PR variants with mutations in positions 48, 82, 84, and 90, often found in drug-resistant PR strains.[8] Detailed kinetic analysis of three chosen inhibitors has even shown somewhat better inhibition of a drug-resistant HIV PR mutant compared with the wild-type enzyme. In the present paper, the structure of wild-type HIV PR complexed with one of these inhibitors, Z-Pns-Phe-Glu-Glu-NH_2 (Z, benzyloxycarbonyl; Pns, phenylnorstatine, (2*R*,3*S*)-3-amino-2-hydroxy-4-phenylbutanoic acid, Figure 1a, termed hereafter KI2), is described. The phenylnorstatine group, an untypical inhibitor moiety, served the purpose of investigating the potential of replacement of the peptide bond with larger groups (the "main chain" between the aromatic groups occupying S1′ and S1 pockets is longer by one carbonyl group compared to common hydroxyethylene or hydroxyethylamine isosteres). This compound inhibits the Val82Ala mutant of HIV PR with a K_i value 0.11 nM, while the wild-type HIV PR inhibition has $K_i = 0.18$ nM.[8]

Since the combinatorial chemistry approach and consecutive primary screening against drug-resistant HIV PR mutants are rather empirical in their nature, only direct structural studies may elucidate subtleties of the inhibitory potential of such developed lead compounds. This paper presents the wild-type HIV PR/phenylnorstatine inhibitor complex structure solved at 1.03 Å, which is the best resolution for HIV PR reported to date. With an excess of inhibitor, the protein/inhibitor crystals grew with an extraordinary diffraction quality, apparently because of the presence of a second inhibitor molecule bound in the crystal lattice as an outer ligand at the protein interface (Brynda et al., manuscript in preparation). Though the compound used for complex formation and crystal growth was a 2:1 mixture of (21*R*,11*S*)- and (21*S*,11*S*)-diastereoisomers, both protease-bound inhibitor molecules had a (21*R*,11*S*)-configuration.

The present paper is focused on two basic structural questions. First, what type of binding makes the (2*R*,3*S*)-phenylnorstatine group, an untypical inhibitor moiety, functional? Second, what structural elements contribute to the unimpaired inhibition of the drug-resistant Val82Ala HIV PR mutant? The first question should raised because the unusual (2*R*,3*S*)-chirality makes the present inhibitor structurally dissimilar to the common (2*S*,3*S*)-phenylnorstatine compounds with their well-described mode of binding of transition-state isosteres to the catalytic center.[9] Regarding the resistance mechanisms in the Val82Ala HIV PR mutant, comparison of wild-type and mutant complex structures was feasible

* To whom correspondence should be addressed. Telephone: +420 20183212. Fax: +420 224310955. E-mail: brynda@img.cas.cz.
† Institute of Molecular Genetics.
‡ Institute of Organic Chemistry and Biochemistry.

10.1021/jm031105q CCC: $27.50
Published on Web 03/10/2004

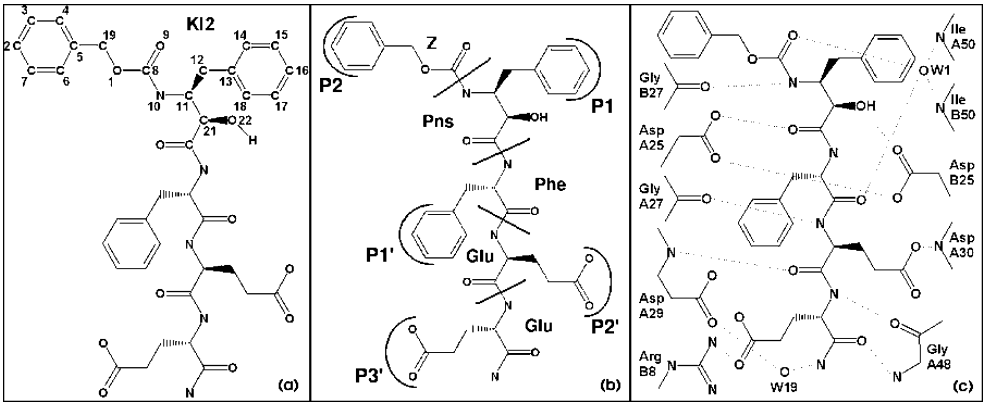

Figure 1. Binding of the inhibitor in the active site. (a) Chemical structure of the inhibitor KI2, where numbering of atoms corresponds to the deposited PDB file (1NH0). (b) Positioning of the inhibitor side chains in the subsites of the active site. The segmentation (bold lines cutting the backbone) was used for energy calculations (see the text). (c) System of hydrogen bonds between inhibitor and the protease active site.

so far for two compounds of different types: Ritonavir itself[10] and a C_2 symmetry based diol inhibitor.[11]

While our solved structure directly shows, in considerable detail, the distinctive pattern of the hydrogen bonding of the present inhibitor to the enzyme catalytic aspartic acid residues, the question of resistance-overcoming mechanisms has been approached using molecular modeling methods and energy calculations.

Results

Inhibitor Binding Mode. The overall scheme of the inhibitor binding is shown in Figure 1b. The inhibitor bound to the active site displays the usual extended conformation, as directed by the occupation of the binding pockets. The S1 pocket consisting of residues Pro A81, Val A82, Ile A84, Gly B27, Gly B49, and Ile B50 contains the aromatic part of the phenylnorstatine group of the inhibitor (Pns group). The S1′ pocket consisting of Gly A27, Gly A49, Arg B8, Pro B81, Val B82, and Ile B84 is occupied by the phenylalanine side chain of the inhibitor. The S2 pocket consisting of Asp B29, Asp B30, Val B32, Ile B47, and Gly B48 contains the aromatic part of the terminal benzyloxycarbonyl group (Z group), while the S2′ pocket consisting of Ala A28, Asp A29, Asp A30, Ile A47, Gly A48, and Ile B50 is occupied by the glutamic acid side chain of the inhibitor. The poor quality of the omit map found for the Z group of the inhibitor in the S2 pocket is best explained by an alternative conformation of the benzyloxy substituent. The S3′ pocket consisting of Ile A47, Gly A48, and Arg B8 contains the terminal glutamic acid group of the inhibitor.

The hydrogen-bonding interactions between the inhibitor and the protein are extensive. The schematic diagram showing the hydrogen bonds is depicted in Figure 1c. While most of the observed hydrogen bonds are common to many pseudopeptide HIV PR inhibitors, the central moiety of the present inhibitor KI2 maintains a unique type of hydrogen bonding. The common hydrogen bonds include interaction of the inhibitor main chain atoms, i.e., O9 oxygen of the Z group with both N Ile A50 and N Ile B50 via one water molecule W1; N10 of the Pns group with O Gly B27; the carbonyl oxygen O Phe I2 with both N Ile A50 and N Ile B50 via water molecule W1; the nitrogen N Glu I3 to O Gly A27; the carbonyl oxygen O Glu I3 to N Asp A29; the nitrogen N Glu I4 to O Gly A48; the carbonyl oxygen O Glu I4 to N Gly A48; and the terminal amide nitrogen to OD2 Asp A29 via a water molecule W19. Also, the carboxylates of both glutamic acid residues of the inhibitor maintain hydrogen bonding (OE1 Glu I3 to OD2 Asp A30, and OE2 Glu I4 to NH2 Arg B8) in their respective binding pockets.

The phenylnorstatine moiety of the inhibitor has two hydrogen-bonding oxygen atoms, i.e., O22 I1 of the central hydroxyl group and the oxygen atom O I1 of the adjacent carbonyl group. The oxygen atom of the carbonyl group (O I1) forms a hydrogen bond with Asp A25, and the oxygen atom of the hydroxyl group (O22 I1) forms a hydrogen bond with Asp B25 (Figure 2). Furthermore, the nitrogen atom of the phenylalanine residue next to the backbone carbonyl group of the inhibitor is remarkably close to the hydrogen-bonding oxygen of Asp B25; the distance of 3.38 Å suggests additional partial hydrogen bonding. The hydrogen atom between OD2 of Asp A25 and OI1 is not directly visible at the actual resolution. Nevertheless, the length of the CG−OD2 bond in the Asp A25 residue is 1.28 Å, significantly more than the parametrized length[12] 1.249-(19) Å indicating protonation of the oxygen atom forming the hydrogen bond with the inhibitor carbonyl group (cf. refs 13 and 14 for the assessment method). In contrast, the bond length CG−OD2 in Asp B25 residue is 1.24 Å, which indicates deprotonation; the hydrogen-bonding hydrogen atom comes from the inhibitor O22 hydroxyl group. The CG−OD1 in the Asp A25 and the Asp B25 residues are 1.24 and 1.25 Å, respectively, indicating that both OD1 oxygen atoms form hydrogen bonds with a shared hydrogen atom (Figure 2).

The observed intermolecular hydrogen bonding does not represent the conventional transition-state analogues where the hydroxyl group of a nonscissile junction is positioned between the two catalytic aspartate carboxyl groups within hydrogen-bonding distance.[1] Complex structures have been determined for two inhibitors that have an (*S*,*S*)-allophenylnorstatine central part, where the hydrogen-bonding hydroxyl group also points between the aspartate carboxyl groups but is positioned markedly out of their plane.[15] The present structure further differs from these. While each oxygen atom of the inhibitor central part maintains separate hydrogen bonding with only one of the carboxyl groups,

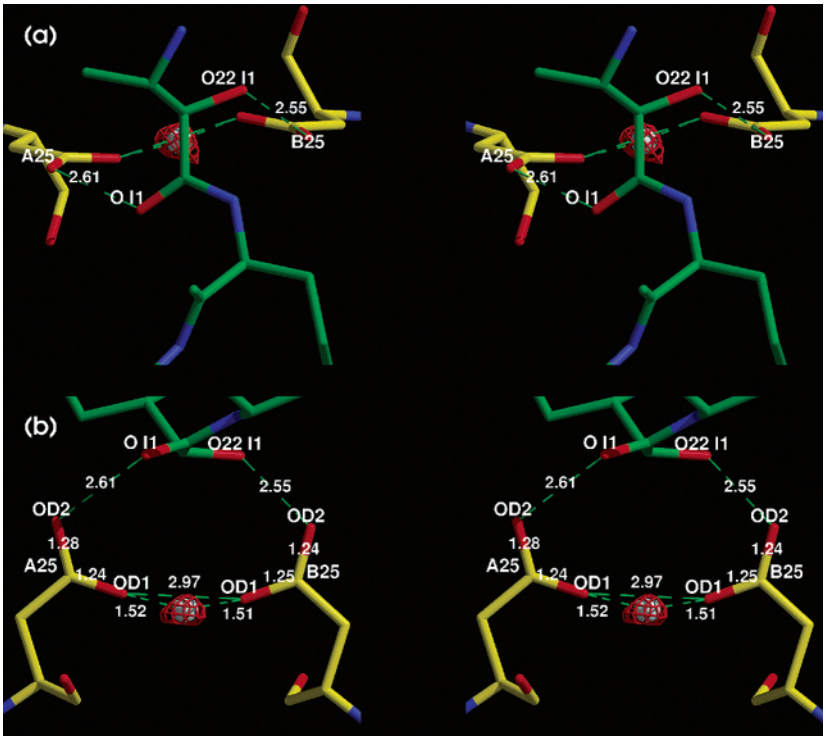

Figure 2. Schematic view of hydrogen bonding of the central part of the inhibitor and the catalytic aspartates. (a) Stereoview along the symmetry axis of the HIV PR dimer. (b) Stereoview perpendicular to the symmetry axis of the HIV PR dimer. Inhibitor carbon atoms are color-coded green, and the protein carbon atoms are color-coded yellow. The hydrogen atom shared by the Asp A25 and Asp B25 residues is shown (white) in the local maximum of the mFo − DFc electron density map (contoured at 2.6σ, red).

the C21−O22 bond has a unique orientation, roughly in the plane of the adjacent carbonyl C═O bond, the torsion angle O−C−C21−O22 being −156° (Figure 2).

To summarize, the present inhibitor KI2 bound in the HIV PR active site displays interactions of its main chain and side chains that are similar to most HIV PR complexes with peptidomimetic inhibitors except for the phenylnorstatine moiety of the KI2 inhibitor that displays unusual positioning relative to the catalytic aspartic acid residues with which it maintains a unique type of hydrogen bonding.

Structural Basis for Unimpaired Inhibition of Val82Ala Mutant. Background information shows that amino acid substitutions in position 82 of HIV PR are frequently associated with drug resistance.[16] Specifically for the Val82Ala mutation, the structural change from the wild-type side chain corresponds to the net loss of two methyl groups from each valine 82 residue, A and B, thus leaving more room in the S1′ and S1 binding pockets for ligand binding. Decreased van der Waals interactions in these pockets can then be considered as the cause of an 8-fold-reduced sensitivity to the drug Ritonavir.[17] Remarkably, KI2 shows an opposite trend: inhibition of the Val82Ala mutant HIV PR is somewhat better than that of the wild-type enzyme.[8] In the present complex structure, an unusual angle of the aromatic "side chain" in the phenylnorstatine moiety (C11−C12−C13 = 105.6°) appears suggestively as an element involved in the difference of the inhibitor binding to the wild-type and mutant HIV PR. A tendency to adopt a normal angle value (which is 113.8° in phenylalanine[12]) could then be expected to improve van der Waals interactions with the mutant enzyme in the larger S1 binding pocket.

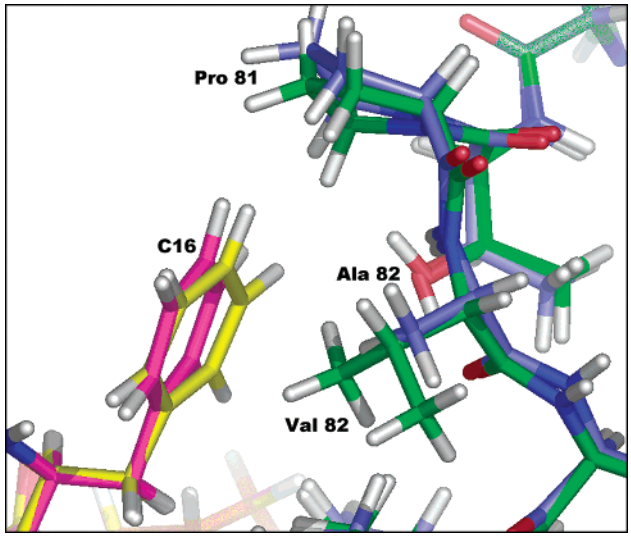

Figure 3. Details of interactions at the P1 subsite. The wild-type protein structure is green, and the modeled Val82Ala mutant is blue. The inhibitor is magenta for the wild-type structure and is yellow for the mutant model.

A more informative view of a structural basis for the unimpaired inhibition of the Val82Ala mutant HIV PR was obtained by a comparison of the present wild-type complex structure with its in silico modeled mutant-enzyme counterpart (see Experimental Procedures). From a structural point of view, the aromatic "side chain" of the phenylnorstatine moiety in the mutant complex adopts a new position in the S1 binding pocket, as depicted in Figure 3. Quantitative data were obtained by molecular-mechanics-based calculations of interaction energies of individual inhibitor segments defined

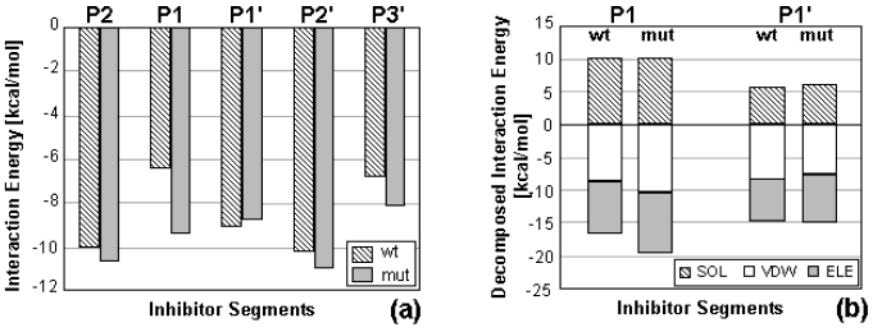

Figure 4. Comparisons of total and decomposed interaction energies calculated for individual subsites. The segmentation of the inhibitor structure is shown in Figure 1b: W, wild-type; MUT, Val82Ala mutant; SOL, solvation; ELE, electrostatic, including hydrogen bonding; VDW, van der Waals.

Table 1. Comparison of Parameters Describing the Inhibitor Binding

	1HXW wt + RIT	1N49 D25N/V82A + RIT	1NH0 wt + KI2	model V82A + KI2
Entire Complex				
inhibitor buried surface area[a] (Å^2)	872.2	812.6	930.6	936.5
inhibitor buried surface area[a] (%)	91.5	83.0	94.9	94.8
gap volume[b] (Å3)	204.2	532.5	164.9	193.5
no. H bonds[c]	9	6	13	14
K_i values[d] (nM)	0.015 ± 0.003	0.12 ± 0.02 5	0.18 ± 0.02	0.11 ± 0.01
S1 Subsite				
inhibitor buried surface area[a] (Å^2)	199.3	179.9	243.1	244.4
inhibitor buried surface area[a] (%)	98.3	84.4	96.6	96.0
gap volume[b] (Å^3)	72.2	179.2	62.5	94.2
no. H bonds[c]	4	3	4	5
S1′ Subsite				
inhibitor buried surface area[a] (Å^2)	124.7	139.7	163.0	168.0
inhibitor buried surface area[a] (%)	95.1	98.5	99.9	99.9
gap volume[b] (Å^3)	55.8	45.1	50.7	57.9
no. H bonds[c]	1	1	1	1

[a] Calculated with program NACCESS.[32] [b] Calculated with program Surfnet.[34] [c] Obtained with program CONTACT (CCP4).[35] [d] As determined in ref 8.

as shown in Figure 1b. The interaction energies of individual inhibitor segments and their respective binding pockets are plotted in the histogram in Figure 4a. While the interaction in S1 is markedly increased with the mutation, the interaction in S1′ is only slightly decreased. A decomposition of the interaction energies into van der Waals, electrostatic (including hydrogen bonding), and solvation energy terms (Figure 4b) shows that the gain in the S1 binding pocket comprises an increase of van der Waals plus electrostatic interactions while the loss in S1′ is contributed by solvation and van der Waals contacts.

The actual loss of the interaction energy in S1′ clearly would not suffice to compensate for the gain found in the S1 binding pocket. The summarized interactions in S1 plus S1′ binding pockets are fully consistent with a better fit of the KI2 structure with the mutant enzyme active site compared to the wild-type. Not surprisingly, the mutation appears almost neutral in regard to the interaction energies calculated for S2, S2′, and S3′ binding pockets (Figure 4a). Such a structural mechanism sharply contrasts with that involved in the Ritonavir resistance, as is apparent from the complex structures solved by others.[10,18] Here, the mutant S1′ shows good occupation by the P1′ aromatic group of Ritonavir but interaction in the S1 is substantially weakened. This loss also involves a shift of the entire Ritonavir molecule in the direction from S1 toward S1′. The shift interferes also with the proper binding of Ritonavir in other binding pockets and thus incrementally weakens the overall Ritonavir interaction. The contrast is illustrated by comparing calculated parameters describing the KI2 and Ritonavir binding to the wild-type and mutant enzyme, listed in Table 1.

Discussion

The hydrogen bonding of the central part of this inhibitor is of a unique type: neither one of the two oxygen atoms maintains hydrogen bonds with both catalytic aspartates, Asp A25 and Asp B25, simultaneously. The carbonyl group (O I1) maintains a hydrogen bond with one catalytic aspartate, while the hydroxyl group (O22 I1) forms a hydrogen bond with the other. The number and distances of hydrogen bonds are comparable to other, more frequently used isosteres, rendering thus the phenylnorstatine group, an untypical inhibitor moiety, a full functionality.

The observed geometry of the inhibitor phenylnorstatine moiety, which is "out of plane" of the catalytic aspartic acid residues, is determined by the (*R*)-configuration on the C21 carbon atom and by the mostly normal occupation of the substrate binding pockets. Surprising in this context is the exclusive presence of the (21*R*,11*S*)-diastereoisomer in the active site (as clearly evidenced by the omit map) despite the fact that the (21*S*,11*S*)-diastereoisomer was also present in an amount sufficient for complex formation before and during the crystal growth. Thus, the empirical finding is that the apparently more tightly bound (*R*,*S*)-diastereoisomer is "extracted" into the enzyme active site,

while it seems difficult a priori to expect its superiority above the (*S*,*S*)-diastereoisomer in view of the existence of tightly bound allophenylnorstatine ((*S*,*S*)-chiral) compounds.[15]

The proton shared by two catalytic aspartic acid residues completes a cyclic hydrogen-bonding element in the interaction of the enzyme and inhibitor. Such a network has not been observed for any other complex of HIV PR. Quite recently, however, the active site protons in complexes of a closely related enzyme, endothiapepsin, with three statine-based inhibitors have been either identified directly in the electron densities or assessed from the carboxyl bond lengths.[14] Distinct protonation states of Asp A25 and Asp B25 in HIV-1 PR/drug complexes have been assessed previously on the basis of NMR evidence.[19] Also, the hydrogen-bonding network we describe here resembles to some extent the cyclic network assessed recently with the crystal structure of an oligosaccharide hydrate.[20] By use of knowledge of the hydrogen donor/acceptor relations (vide supra), the cyclic hydrogen-bonding element of HIV PR may be classified as a homodromic hexagon.

Though not originally "tailored" to inhibit the Ritonavir-resistant Val82Ala HIV PR mutant, the solved complex wild-type HIV PR structure and in silico calculations show that KI2 has specific characteristics to serve such a purpose. Owing to the relatively long "main chain" of the critical central part of KI2, the occupation of the wild-type S1 pocket requires a deformation, as though the wild-type pocket were too "tight" for the respective aromatic "side chain". All calculated parameters show that the strain is relieved with the Val82Ala mutation. Such findings can be valued as a special case of the contribution to the original ideas on the structural mechanisms of the HIV PR drug resistance.[17]

Conclusions

This paper presents the structure of the HIV-1 protease in complex with (2*R*,3*S*)-phenylnorstatine compound Z-Pns-Phe-Glu-Glu-NH_2 (KI2), determined at the highest resolution so far reported for any HIV protease complex (1.03 Å). The observed details of structural elements found excellently match the earlier findings on the inhibitor properties.[8] First, the mostly normal occupation of the HIV PR binding pockets by the inhibitor "side chains" and the apparently stable hydrogen bonding of the central phenylnorstatine moiety to the catalytic aspartate residues correspond to the subnanomolar inhibition constant. Second, the solved wild-type complex structure also gives clues to explain unimpaired inhibition of the Ritonavir resistance conferring mutant. While the solved structure reveals a strained conformation of the aromatic "side chain" of phenylnorstatine moiety in the wild-type S1 binding pocket, this deformation is not present in our model of the inhibitor in the "looser" Val82Ala-mutated S1 binding pocket. Naturally, such a structural mechanism is absent with Ritonavir and other inhibitors.[11,21] Because of a shorter main chain, Ritonavir cannot form a proper binding in the Val82Ala mutant S1 and S1′ binding pockets simultaneously.

Taken together, these results further validate the particular approach to overcome the HIV PR drug resistance by employing extended central parts in the design of lead compounds combined with their primary screening against drug-resistant HIV PR mutants.

Experimental Procedures

Crystallization. Inhibitor Z-Pns-Phe-Glu-Glu-NH_2, (Pns = (2*RS*,3*S*)-3-amino-2-hydroxy-4-phenylbutanoic acid) was synthesized on a Rink amide MBHA resin using the Fmoc/*tert*-butyl-HOBt/DIC strategy. Peptide cleaved from the resin was purified by HPLC and characterized by amino acid analysis and FAB MS, as published previously.[8]

HIV-1 PR (wild-type, Bru isolate) used for crystallization was prepared as described previously.[22] The complex was prepared by admixing the HIV-1 PR with a 6-fold molar excess of the inhibitor (from a 10 mM stock solution in dimethyl sulfoxide). For crystallization experiments, the complex was transferred to a buffer solution containing 10 mM sodium acetate, pH 5.6, 0.05% 2-mercaptoethanol, and 1 mM ethylenediaminetetraacetic acid (EDTA), and the mixture was concentrated by means of ultrafiltration using Centricon-10 (Millipore). Crystallization trials were performed by the hanging-drop technique, and the best crystals were obtained under the following conditions: 1 μL of the reservoir solution (50 mM MES, pH 6.5, 2.4 M ammonium sulfate) was mixed with 2 μL of the solution containing the HIV-1 PR/inhibitor complex at a concentration of 2.2 mg/mL and was allowed to equilibrate over 1 mL of the reservoir solution at 18 °C. After several days, crystals with the dimensions 0.2 mm × 0.2 mm × 0.3 mm appeared.

X-ray Data Collection. Crystals were soaked in the reservoir solution with 20% (v/v) glycerol and transferred into liquid nitrogen. Diffraction data were collected using synchrotron radiation, wavelength of 0.93 Å (ESRF Grenoble, ID14-2), and ADSC Q4 CCD based detector at 100 K (Oxford Cryosystem). Two crystals were measured: crystal 1 diffracted up to 1.03 Å, data were collected in two passes, a high-resolution pass comprising data from 10.0 to 1.03 Å, and a low-resolution pass comprising data from 55.0 to 1.9 Å. Data were measured with 1° oscillation, and the exposure time was 8 and 1 s, respectively. Data for the second crystal were measured with 0.2° oscillation, and the exposure time was 2 and 1 s, respectively. All data sets were integrated by XDS[23] and scaled by XSCALE.[24] The small slices technique gave better R_{meas} values. However, the best data set was obtained by scaling all data sets together. The data collection statistics are shown in Table 2.

Structure Determination, Refinement, and Analysis. The HIV-1 PR/inhibitor structure was solved by molecular replacement using the EPMR program.[25] HIV-1 PR from a complex structure (PDB code: 1VIK[26]) was used as a search model. Structure factors in the 15−4 Å resolution range were used for both the rotational and translational searches. The solution yielded a correlation coefficient of 0.553 and an *R* factor of 45.3%. After the initial rigid-body refinement, using the CNS program[27] at 50−1.6 Å resolution (monomers allowed to move independently), the *R* factor and R_{free} values fell to 42.7% and 43.6%, respectively. Further refinement of the model containing only HIV-1 PR was carried out with CNS using the simulated annealing protocol.[27] The R_{free} factor[28] was used to monitor the progress of the refinement by omitting 2.5% of the data (2164 reflections), randomly chosen. Building of the inhibitor was performed using XtalView.[29]

At this stage, a model of the inhibitor molecule was built in the enzyme active site. After repeated cycles of the refinement, the model of an inhibitor bound at the protein interface was built by fitting it into difference electron density maps. The completed model was then refined by conjugate gradient least-squares methods against structure factors using SHELXL-97.[30] Binning of the *R* value by resolution showed that the bulk solvent correction, as implemented in SHELXL-97, did not describe the low-resolution data well. Therefore, low-resolution cutoff at 6 Å was applied.

Twenty amino acids in multiple conformations for protein and "inhibitor side chains" were introduced for residues

Table 2. Crystallographic Statistics

parameter	
Data Collection Statistics	
space group	*P*212121
unit cell	
a (Å)	28.85
b (Å)	66.52
c (Å)	93.00
diffraction limits (Å)	54.1−1.03
no. of measured reflections	872 620
no. of unique reflections	88 784
average $I/\sigma(I)$ [a]	10.5 (1.85)
R_{sym} (%)[a]	7.8 (37.9)
completeness (%)[a]	99.0 (93.3)
Wilson *B* factor (Å^2)	7.9
Refinement Statistics	
R factor (%)	13.0
R-free factor (%)	16.5
non-hydrogen atoms	1937
non-hydrogen atoms in inhibitors	106
heterogeneous atoms	15
water molecules	233
reflections used in refinement	86 020
reflections in test set	2205
rmsd from ideal bond distances (Å)	0.016
rmsd from ideal valence angle values (deg)	0.036

[a] Values in parentheses correspond to the last resolution shell (1.06−1.03 Å).

exhibiting alternative conformations in 1.5σ 2mFo − DFc and 3σ mFo − DFc electron density maps. During further refinement, anisotropic displacement parameters for protein and active site inhibitor atoms were introduced and the refinement using SHELXL-97 was continued. Next, anisotropic displacement parameters of atoms of outer ligand and solvent molecules were added to the model.

Hydrogen atoms of amino acids, placed according to stereochemistry, further reduced the R_{work} and R_{free} values. At the end of the refinement, a round of blocked full-matrix least-squares refinement was performed using all reflections (including those previously used for R_{free}) to obtain a proper estimate of standard deviations of all refined parameters.

The stereochemical quality of the model was controlled with PROCHECK.[31] Atomic coordinates have been deposited into the Protein Data Bank, PDB code 1NH0. The refinement statistics is shown in Table 2.

Buried surface areas were calculated using the program NACCESS,[32] an implementation of the Lee and Richards algorithm.[33] The default values (probe radius, 1.4 Å; *z*-slices, 0.05 Å; van der Waals radii) were used in the calculations. The volume of the gaps between the inhibitor and the protease was calculated using the program SURFNET[34] (maximal and minimal radii of 4.0 and 1.0 Å, respectively). Hydrogen bonds (≤3.2 Å) and van der Waals contacts (≤4.0 Å) were analyzed by the program CONTACT (CCP4).[35]

Molecular Modeling. The simulations and energy analyses were carried out in AMBER 7.0.[36] Structure manipulation was performed with INSIGHT II 2000.[37] Charges for the inhibitor atoms were obtained from quantum mechanical calculations using Gaussian 98, revision A6.[39]

Hydrogen atoms were added to the crystal structure of the wild-type HIV protease/inhibitor complex. The protonation of the active site aspartic acid residues was done according to the findings of the X-ray analysis (this work). The Val82Ala mutant was created by replacing the two valine side chains in the wild-type protease with alanine. The model included the crystallographically determined water molecules.

In the simulations, the biomolecular force field ff99[39] was used for the protease and general AMBER force field (gaff)[36] parameters were used for the inhibitor. Partial charges for the inhibitor atoms were determined by fitting electrostatic potential calculated at the HF/6-31G* level. In the wild-type complex, we optimized hydrogen atom positions only. In the mutant, we first relaxed the hydrogen atoms followed by 10 000 cycles of minimization in the neighborhood of the mutated residue (residues 23, 80−84 from both protease monomers) plus all atoms of the inhibitor.

Using the resulting structures, we calculated protease−inhibitor interaction energies with an MM-GBSA approach (molecular mechanics generalized Born surface area).[40] Energy terms were separated into van der Waals, electrostatic, and solvation terms. For the purposes of decomposition, the inhibitor structure was split into amino-acid-like segments (from P2 to P3′ in Figure 1b).

Acknowledgment. This work was supported by grants from the Grant Agency of the Czech Republic (Grant Nos. 203/98/K023, 203/02/P095, and 203/02/0405), from the Czech Ministry of Public Health (Grant No. NI/6339-3), from the Czech Ministry of Education (Grant No. LN00A032), and from the European Commission 5th Framework (Grant No. QLRT-2000-02360). The work of J.K. was carried out under Research Project No. Z4 055 905.

References

(1) Wlodawer, A.; Vondrasek, J. Inhibitors of HIV-1 Protease: A major success of structure-assisted drug design. *Annu. Rev. Biophys. Biomol. Struct.* **1998**, *27*, 249−284.
(2) Lescar, J.; Brynda, J.; Rezacova, P.; Stouracova, R.; Riottot, M.-M.; Chitarra, V.; Fabry, M.; Horejsi, M.; Sedlacek, J.; Bentley, G. A. Inhibition of the HIV-1 and HIV-2 proteases by a monoclonal antibody. *Protein Sci.* **1999**, *8*, 2686−2696.
(3) Weber, J.; Mesters, J. R.; Lepsik, M.; Prejdova, J.; Svec, M.; Sponarova, J.; Mlcochova, P.; Skalicka, K.; Strisovsky, K.; Uhlikova, T.; Soucek, M.; Machala, L.; Stankova, M.; Vondrasek, J.; Klimkait, T.; Kraeusslich, H. G.; Hilgenfeld, R.; Konvalinka, J. Unusual binding mode of an HIV-1 protease inhibitor explains its potency against multi-drug-resistant virus strains. *J. Mol. Biol.* **2002**, *324*, 739−754.
(4) Dohnalek, J.; Hasek, J.; Duskova, J.; Petrokova, H.; Hradilek, M.; Soucek, M.; Konvalinka, J.; Brynda, J.; Sedlacek, J.; Fabry, M. Hydroxyethylamine isostere of an HIV-1 protease inhibitor prefers its amine to the hydroxy group in binding to catalytic aspartates. A synchrotron study of HIV-1 protease in complex with a peptidomimetic inhibitor. *J. Med. Chem.* **2002**, *45*, 1432−1438.
(5) Yoshimura, K.; Kato, R.; Kavlick, M. F.; Nguyen, A.; Maroun, V.; Maeda, K.; Hussain, K. A.; Ghosh, A. K.; Gulnik, S. V.; Erickson, J. W.; Mitsuya, H. A potent human immunodeficiency virus type 1 protease inhibitor, UIC-94003 (TMC-126), and selection of a novel (A28S) mutation in the protease active site. *J. Virol.* **2002**, *76*, 1349−1358.
(6) Yoshimura, K.; Kato, R.; Yusa, K.; Kavlick, M. F.; Maroun, V.; Nguyen, A.; Mimoto, T.; Ueno, T.; Shintani, M.; Falloon, J.; Masur, H.; Hayashi, H.; Erickson, J.; Mitsuya, H. JE-2147: A dipeptide protease inhibitor (PI) that potently inhibits multi-PI-resistant HIV-1. *Proc. Natl. Acad. Sci. U.S.A.* **1999**, *96*, 8675−8680.
(7) Houghten, R. A.; Pinilla, C.; Blondelle, S. E.; Appel, J. R.; Dooley, C. T.; Cuervo, J. H. Generation and use of synthetic peptide combinatorial libraries for basic research and drug discovery. *Nature* **1991**, *354*, 84−86.
(8) Rinnova, M.; Hradilek, M.; Barinka, C.; Weber, J.; Soucek, M.; Vondrasek, J.; Klimkait, T.; Konvalinka, J. A picomolar inhibitor of resistant strains of human immunodeficiency virus protease identified by a combinatorial approach. *Arch. Biochem. Biophys.* **2000**, *382*, 22−30.
(9) Kiso, Y.; Matsumoto, H.; Mizumoto, S.; Kimura, T.; Fujiwara, Y.; Akaji, K. Small dipeptide-based HIV protease inhibitors containing the hydroxymethylcarbonyl isostere as an ideal transition-state mimic. *Biopolymers* **1999**, *51*, 59−68.
(10) Prabu-Jeyabalan, M.; Nalivaika, E. A.; King, N. M.; Schiffer, C. A. Viability of a drug-resistant human immunodeficiency virus type 1 protease variant: structural insights for better antiviral therapy. *J. Virol.* **2003**, *77*, 1306−1315.
(11) Baldwin, E. T.; Bhat, T. N.; Liu, B.; Pattabiraman, N.; Erickson, J. W. Structural basis of drug resistance for the V82A mutant of HIV-1 proteinase. *Nat. Struct. Biol.* **1995**, *2*, 244−249.
(12) Engh, R. A.; Huber, R. Accurate bond and angle parameters for X-ray protein structure refinement. *Acta Crystallogr. A* **1991**, *47*, 392−400.
(13) Wlodawer, A.; Li, M.; Gustchina, A.; Dauter, Z.; Uchida, K.; Oyama, H.; Goldfarb, N. E.; Dunn, B. M.; Oda, K. Inhibitor complexes of the *Pseudomonas* serine-carboxyl proteinase. *Biochemistry* **2001**, *40*, 15602−15611.

(14) Coates, L.; Erskine, P. T.; Crump, M. P.; Wood, S. P.; Cooper, J. B. Five atomic resolution structures of endothiapepsin inhibitor complexes: implications for the aspartic proteinase mechanism. *J. Mol. Biol.* **2002**, *318*, 1405−1415.
(15) Reiling, K. K.; Endres, N. F.; Dauber, D. S.; Craik, C. S.; Stroud, R. M. Anisotropic Dynamics of the Je-2147-HIV protease complex: drug resistance and thermodynamic binding mode examined in a 1.09 Å structure. *Biochemistry* **2002**, *41*, 4582−4594.
(16) D'Aquila, R. T.; Schapiro, J. M.; Brun-Vezinet, F.; Clotet, B.; Conway, B.; Demeter, L. M.; Grant, R. M.; Johnson, V. A.; Kuritzkes, D. R.; Loveday, C.; Shafer, R. W.; Richman, D. D. Drug resistance mutations in HIV-1. *Top. HIV Med.* **2002**, *10*, 11−19.
(17) Erickson, J. W.; Burt, S. K. Structural mechanisms of HIV drug resistance. *Annu. Rev. Pharmacol. Toxicol.* **1996**, *36*, 545−571.
(18) Kempf, D. J.; Marsh, K. C.; Denissen, J. F.; McDonald, E.; Vasavanonda, S.; Flentge, C. A.; Green, B. E.; Fino, L.; Park, C. H.; Kong, X. P.; et al. ABT-538 is a potent inhibitor of human immunodeficiency virus protease and has high oral bioavailability in humans. *Proc. Natl. Acad. Sci. U.S.A.* **1995**, *92*, 2484−2489.
(19) Wang, Y. X.; Freedberg, D. I.; Yamazaki, T.; Wingfield, P. T.; Stahl, S. J.; Kaufman, J. D.; Kiso, Y.; Torchia, D. A. Solution NMR evidence that the HIV-1 protease catalytic aspartyl groups have different ionization states in the complex formed with the asymmetric drug KNI-272. *Biochemistry* **1996**, *35*, 9945−9950.
(20) Imamura, K.; Nimz, O.; Jacob, J.; Myles, D.; Mason, S. A.; Kitamura, S.; Aree, T.; Saenger, W. Hydrogen-bond network in cyclodecaamylose hydrate at 20 K; neutron diffraction study of novel structural motifs band-flip and kink in alpha-(1→4)-D-glucoside oligosaccharides. *Acta Crystallogr. B* **2001**, *57*, 833−841.
(21) Baldwin, E. T.; Bhat, T. N.; Gulnik, S.; Liu, B.; Topol, I. A.; Kiso, Y.; Mimoto, T.; Mitsuya, H.; Erickson, J. W. Structure of HIV-1 protease with KNI-272, a tight-binding transition-state analog containing allophenylnorstatine. *Structure* **1995**, *3*, 581−590.
(22) Sedlacek, J.; Fabry, M.; Horejsi, M.; Brynda, J.; Luftig, R. B.; Majer, P. A rapid screening method for biological activity of human immunodeficiency virus proteinase inhibitors by using a recombinant DNA-derived bacterial system. *Anal. Biochem.* **1993**, *215*, 306−309.
(23) Kabsch, W. XDS. In *International Tables for Crystallography*,, 1st ed.; Rossmann, M. G., Arnold, E., Eds.; Kluwer Academic Publishers: Dordrecht, The Netherlands, 2001; Vol. F, pp 730−734.
(24) Kabsch, W. Integration, scaling, space-group assignment and post refinement. In *International Tables for Crystallography*,, 1st ed.; Rossmann, M. G., Arnold, E., Eds.; Kluwer Academic Publishers: Dordrecht, The Netherlands, 2001; Vol. F, pp 218−224.
(25) Kissinger, C. R.; Gehlhaar, D. K.; Fogel, D. B. Rapid automated molecular replacement by evolutionary search. *Acta Crystallogr. D* **1999**, *55*, 484−491.
(26) Lange-Savage, G.; Berchtold, H.; Liesum, A.; Budt, K. H.; Peyman, A.; Knolle, J.; Sedlacek, J.; Fabry, M.; Hilgenfeld, R. Structure of HOE/BAY 793 complexed to human immunodeficiency virus (HIV-1) protease in two different crystal forms—structure/function relationship and influence of crystal packing. *Eur. J. Biochem.* **1997**, *248*, 313−322.
(27) Brunger, A. T.; Adams, P. D.; Clore, G. M.; Delano, W. L.; Gros, P.; Grosse-Kunstleve, R. W.; Jiang, J.-S.; Kuszewski, J.; Nilges, M.; Pannu, N. S.; Read, R. J.; Rice, L. M.; Simonson, T.; Warren, G. L. Crystallography and NMR system: new software suite for macromolecular structure determination. *Acta Crystallogr. D* **1998**, *54*, 905−921.
(28) Brunger, A. T. Free *R* value: a novel statistical quantity for assessing the accuracy of crystal structures. *Nature* **1992**, *355*, 472−475.
(29) McRee, D. E. XtalView/Xfit—A versatile program for manipulating atomic coordinates and electron density. *J. Struct. Biol.* **1999**, *125*, 156−165.
(30) Sheldrick, G. M.; Schneider, T. R. SHELXL: high-resolution refinement. *Methods Enzymol.* **1997**, *277*, 319−343.
(31) Laskowski, R. A.; McArthur, M. W.; Moss, D. S.; Thornton, J. M. PROCHECK: a program to check the stereochemical quality of protein structures. *J. Appl. Crystallogr.* **1993**, *26*, 283−291.
(32) Hubbard, S. J.; Thornton, J. M. *NACCESS* (Computer Program); Department of Biochemistry and Molecular Biology, University College London: London, 1993.
(33) Lee, B.; Richards, F. M. The interpretation of protein structures: Estimation of static accessibility. *J. Mol. Biol.* **1971**, *55*, 379−400.
(34) Laskowski, R. A. SURFNET: A program for visualizing molecular surfaces, cavities and intermolecular interactions. *J. Mol. Graphics* **1995**, *13*, 323−330.
(35) Collaborative Computational Project, Number 4. The CCP4 suite: programs for protein crystallography. *Acta Crystallogr. D* **1994**, *50*, 760−763.
(36) Case, D. A.; Pearlman, D. A.; Caldwell, J. W.; Cheatham, T. E., III; Wang, J.; Ross, W. S.; Simmerling, C. L.; Darden, T. A.; Merz, K. M.; Stanton, R. V.; Cheng, A. L.; Vincent, J. J.; Crowley, M.; Tsui, V.; Gohlke, H.; Radmer, R. J.; Duan, Y.; Pitera, J.; Massova, I.; Seibel, G. L.; Singh, U. C.; Weiner, P. K.; Kollman, P. A. *AMBER 7*; University of California, San Francisco, 2002.
(37) *InsightII 2000*; Molecular Simulations Inc.: San Diego, CA, 2000.
(38) Frisch, M. J.; Trucks, G. W.; Schlegel, H. B.; Scuseria, G. E.; Robb, M. A.; Cheeseman, J. R.; Zakrzewski, V. G.; Montgomery, J. A., Jr.; Stratmann, R. E.; Burant, J. C.; Dapprich, S.; Millam, J. M.; Daniels, A. D.; Kudin, K. N.; Strain, M. C.; Farkas, O.; Tomasi, J.; Barone, V.; Cossi, M.; Cammi, R.; Mennucci, B.; Pomelli, C.; Adamo, C.; Clifford, S.; Ochterski, J.; Petersson, G. A.; Ayala, P. Y.; Cui, Q.; Morokuma, K.; Malick, D. K.; Rabuck, A. D.; Raghavachari, K.; Foresman, J. B.; Cioslowski, J.; Ortiz, J. V.; Stefanov, B. B.; Liu, G.; Liashenko, A.; Piskorz, P.; Komaromi, I.; Gomperts, R.; Martin, R. L.; Fox, D. J.; Keith, T.; Al-Laham, M. A.; Peng, C. Y.; Nanayakkara, A.; Gonzalez, C.; Challacombe, M.; Gill, P. M. W.; Johnson, B. G.; Chen, W.; Wong, M. W.; Andres, J. L.; Head-Gordon, M.; Replogle, E. S.; Pople, J. A. *Gaussian 98*, revision A.6; Gaussian, Inc.: Pittsburgh, PA, 1998.
(39) Wang, J. M.; Cieplak, P.; Kollman, P. A. How well does a restrained electrostatic potential (RESP) model perform in calculating conformational energies of organic and biological molecules? *J. Comput. Chem.* **2000**, *21*, 1049−1074.
(40) Massova, I.; Kollman, P. A. Combined molecular mechanical and continuum solvent approach (MM-PBSA/GBSA) to predict ligand binding. *Perspect. Drug Discovery Des.* **2000**, *18*, 113−135.

JM031105Q